# A Comparative Study between Spin-Transfer-Torque (STT) and Spin-Hall-Effect (SHE) Switching Mechanisms in PMTJ using SPICE

Ibrahim Ahmed, Zhengyang Zhao, Meghna G. Mankalale, Sachin S. Sapatnekar, Jian-Ping Wang, and Chris H. Kim

*Abstract*—**Spin transfer torque magnetoresistive random access memory (STT-MRAM) is the leading candidate for spin-based memories. Nevertheless, the high write energy and read disturbance of STT-MRAM motivated researchers to find other solutions. Spin Hall effect (SHE) based MRAM is an alternative for STT-MRAM which also provides non-volatility, zero leakage, and competitive area per bit, but with a lower write current. This work focuses on a systematic performance analysis of these two proposed memory solutions. SHE requires an external field to deterministically switch perpendicular magnetic anisotropy (PMA) MTJ. A previous experiment showed SHE can switch composite MTJ containing an in-plane layer without any field. In this work, both traditional and composite MTJ structures are modeled in SPICE which can reproduce realistic MTJ characteristics with user-defined input parameters. This self-contained model is used to compare the write energy and delay of STT-MRAM and SHE-MRAM for various write schemes including thermal fluctuation. Our simulations show, compared to STT-MRAM, SHE-MRAM improves the write delay and energy by 8× and 7×, respectively. Based on our extensive analysis incorporating the latest advances in magnetic materials and device technology, we predict that SHE-MRAM is a feasible low energy memory solution for future computing systems.**

*Index Terms*—**Spintronics, STT-MRAM, SHE-MRAM, Composite MTJ, MTJ model, Initial Angle, Thermal Fluctuation.**

## I. Introduction

CMOS technology defined the way we create, store, transform, and transmit information in the digital age. Moore's law of scaling continued to improve information technology till today. However, we are now approaching fundamental area, power and performance limitations of CMOS as we reach the physical limits of silicon. Spintronic devices are potential candidates for a low-power alternative to CMOS technology to stretch Moore's law beyond CMOS. There have been many proposals for spin based logic devices, such as all spin logic (ASL) [1], domain wall logic (DWL) [2], nanomagnet logic (NML) [3], voltage controlled logic [4]. However, the most mature application of spintronic devices so far is in memory applications.

Magnetic tunnel junction (MTJ) based spin transfer torque magnetic random access memory (STT-MRAM) is considered the most practical spintronic device that can be used in the next-generation microprocessor systems [5]–[9]. STT-MRAM has shown some benefits over the conventional SRAM-based

memory, for example, the non-volatility, zero static power, and compact bit-cell size [10]–[12]. STT-MRAM is predicted to outperform SRAM for higher level cache memory applications by reducing the overall delay and power with shorter global interconnects [13]. However, the key challenge of STT-MRAM is the high write energy associated with the retention time required for memory applications. There is also a trade-off between read speed and disturbance. Spin Hall effect (SHE), a recently experimentally demonstrated phenomenon, is predicted to be an efficient switching mechanism. SHE-MRAM provides the benefits of STT-MRAM and has decoupled read and write path [14] [15]. SHE-MRAM has also shown a faster read with a smaller read disturbance [16].

In this work, we systemically analyze the performance of STT-MRAM and SHE-MRAM considering the probabilistic switching due to thermal fluctuation for various possible write schemes for both traditional and composite [17] MTJ structures using a self-contained MRAM model for STT, SHE, and SHE-assisted STT. The paper is organized as following. First the background and key physics to model STT-MRAM and SHE-MRAM are described in Section II. Next, the SPICE model framework is explained in Section III. Section IV contains the performance analysis of STT-MRAM and SHE-MRAM using the proposed model, and finally, Section V concludes the paper.

## II. Background and Key Physics

### A. Magnetic Anisotropy

The directional dependence of the magnetic properties of a material is known as magnetic anisotropy (MA). MA provides an easy axis along which the magnetization can easily be aligned. Based on the source of the MA and the alignment of easy axis, there are a few possible combinations for MTJ. In-plane magnetic anisotropy (IMA) MTJs (IMTJs) have their easy axis aligned along the plane of the magnet, as shown in Fig. 1(a). The source of such MA is shape anisotropy. The magnetization, **M**, aligns with the longest dimension as the demagnetizing field, **H$_d$**, is stronger along the shorter dimension. The strongest **H$_d$** in an IMTJ is along the z-axis which keeps the easy axis in the x-y plane. The shape anisotropy field, ($H_{K,shape}$) is as follows:

$$H_{K,shape} = 4\pi(N_{dx} - N_{dy})M_s \qquad (1)$$

Here, $M_s$ is the saturation magnetization and $N_d = [N_{dx}, N_{dy}, N_{dz}]$ is the demagnetizing factor of the free layer.
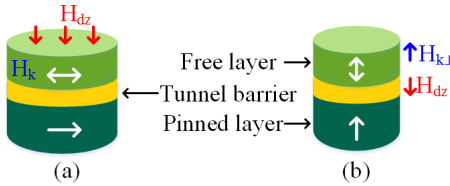
All the authors are with the Department of Electrical and Computer Engineering, University of Minnesota, Minneapolis, MN, USA (email: ahmed589@umn.edu)

Fig. 1: Magnetization configuration of (a) in-plane MTJ and (b) perpendicular MTJ



Fig. 2: Bidirectional switching of spin transfer torque
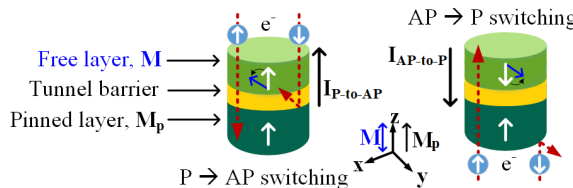


Fig. 3: Bidirectional switching of spin Hall effect

The perpendicular MA (PMA) based MTJs (PMTJs) have an easy axis aligned along the z-axis as shown in Fig. 1(b). The source of PMA can be either interface or crystalline anisotropy. Interface anisotropy based MTJ (IPMTJ) is achieved using a ferromagnetic electrode interfaced with a tunnel barrier or heavy metal where ferromagnetic layer is thinner than a critical thickness ($t_c$), for example, CoFeB interfaced with MgO layer [18]. Crystalline anisotropy based MTJ (CPMTJ) can be designed with a high crystal anisotropy ($K_u$) material, for example, CoPt, FePd, Heusler alloys. The effective perpendicular anisotropy field, ($H_{K\perp0}$) is expressed as follows:

$$H_{K\perp0} = H_{K\perp} - H_{dz} = 2K_\perp/M_s - 4\pi N_{dz}M_s \quad (2)$$

Here, $K_\perp$ is the $K_u$ of crystalline perpendicular material, and for interface anisotropy, $K_\perp = 2\pi M_s^2 t_c/t_F$, where $t_F$ is the thickness of free layer [18].

### B. MTJ Switching Mechanism

We focus on three MTJ switching mechanisms: spin transfer torque (STT), spin Hall effect (SHE), and SHE-assisted STT. In addition, we take the effect of external field derived from an independent source or from a modified device structure.

*1) Spin Transfer Torque:* Charge current passing through MTJ pinned layer becomes spin polarized and exerts a torque on the free-layer. The direction of the applied current and magnetization of the pinned layer, $\mathbf{M_p}$, determines the direction of generated torque. A large enough torque can switch the free layer magnetization, $\mathbf{M}$, as shown in Fig. 2. As $\mathbf{M_p}$ is fixed, a bidirectional current is required to switch the free layer states.

*2) Spin Hall Effect:* A charge current in the heavy metals, such as Ta, W, Pt, creates a spin current in the transverse direction which is polarized along the in-plane direction, $\boldsymbol{\sigma}_{SHE}$. This effect is known as the SHE which arises from the spin-orbit interactions [15]. SHE can provide large enough torque on the adjacent MTJ free layer to switch the magnetization [14]. Traditional SHE devices comprised of a heavy spin Hall metal (SHM) and an MTJ grown on top of the metal [14]
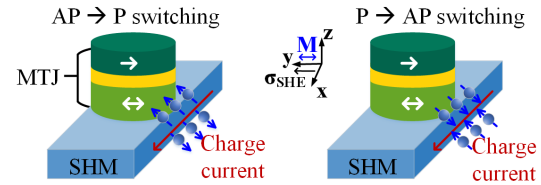
[15]. A bidirectional current in SHM determines the switching direction of the free-layer as shown in Fig. 3.

SHE can naturally switch the magnetization in IMTJs [14] [15] as shown in Fig. 4(a) since $\boldsymbol{\sigma}_{SHE}$ is (anti-)parallel to the free layer magnetization, $\mathbf{M}$. However, for PMA, $\boldsymbol{\sigma}_{SHE}$ is perpendicular to $\mathbf{M}$. As a result, SHE can bring the PMA free layer up to in-plane level, but cannot deterministically switch it as shown in Fig. 4(b). An external field is required to break the symmetry for deterministic switching of PMA magnetization [14] [15] [19] [20] as shown in Fig. 4(c).

### C. Dynamic Motion of Magnetization

The effective field experienced by the free layer in the absence of any external field, $\mathbf{H}_{eff0-}$, is governed by demagnetization field along z-axis, $\mathbf{H}_d$.

$$\mathbf{H}_{eff0-}(t) = \mathbf{H}_d = -4\pi M_s[N_{dx}M_x(t), N_{dy}M_y(t), N_{dz}M_z(t)] \quad (3)$$

The effective field of a PMA MTJ, $\mathbf{H}_{eff0\perp}(t)$ is a combination of both $\mathbf{H}_d$ and $K_\perp$.

$$\mathbf{H}_{eff0\perp}(t) = -4\pi M_s[N_{dx}M_x(t), N_{dy}M_y(t), N_{dz}M_z(t)]$$
$$+ \left[0, 0, \left(\frac{2K_\perp}{M_s}\right)M_z(t)\right] \quad (4)$$

The Landau-Lifshitz-Gilbert (LLG) equation is a differential equation that describes the precessional motion of a time-varying magnetization vector, $\mathbf{M}(t) = [M_x(t), M_y(t), M_z(t)]$. Under an STT current density, $J_{STT}$, and SHE current with density, $J_{SHM}$, it is given by:

$$\frac{1+\alpha^2}{\gamma} \cdot \frac{d\mathbf{M}}{dt} = -\mathbf{M} \times \mathbf{H}_{eff} - \alpha \cdot \mathbf{M} \times (\mathbf{M} \times \mathbf{H}_{eff})$$
$$+ \zeta_{STT} \cdot \mathbf{M} \times (\mathbf{M} \times \mathbf{M}_p) \quad (5)$$
$$+ \zeta_{SHE} \cdot \mathbf{M} \times (\mathbf{M} \times \boldsymbol{\sigma}_{SHE})$$

$$\text{Where } \zeta_{STT} = \frac{\hbar P J_{MTJ}}{2et_f M_s}, \zeta_{SHE} = \frac{\hbar\theta_{SHE}J_{SHM}}{2et_f M_s}, \quad (6)$$

$$\mathbf{H}_{eff} = \mathbf{H}_{eff0} + \mathbf{H}_{app} \quad (7)$$

Here, $\gamma$ is gyromagnetic ratio, $\alpha$ is damping constant, $\hbar$ is reduced Plank's constant, $e$ is charge of an electron, $P$ is spin polarization factor and $t_f$ is thickness of MTJ free layer, spin Hall angle, $\theta_{SHE}$ is a geometry dependent parameter, $\boldsymbol{\sigma}_{SHE}$ is the spin polarization direction, and $\mathbf{H}_{eff}$ incorporates the external field, $\mathbf{H}_{app}$. When there is no applied field, $\mathbf{H}_{app} = 0$.

The equation (5) provides a complete representation of a system describing STT-only, SHE-only, and SHE-assisted STT switching with and without the presence of an external field. A summary of different variables in (5) is shown in Table I.
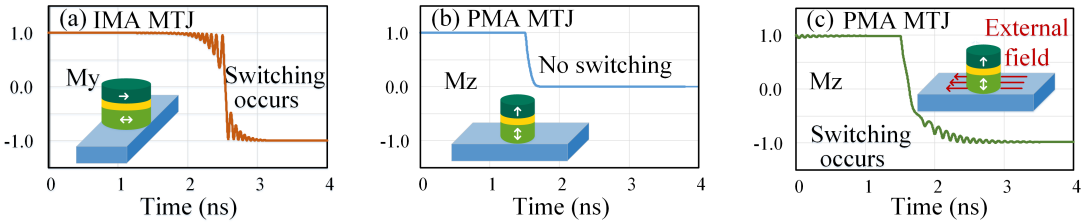
Fig. 4: SHE switching of (a) in-plane MTJ, (b) perpendicular MTJ, (c) perpendicular MTJ with field

The magnetization reversal with STT and SHE are shown in Fig. 5. The STT is proportional to the sin function of angle between $\mathbf{M}$ and $\mathbf{M}_p$ which is initially very small. Thus, it requires a longer time for STT to begin the reversal, but it can switch quickly after initiation. SHE depends on the angle between $\sigma_{SHE}$ and $\mathbf{M}$ which are initially perpendicular to each other. Hence, SHE can quickly bring the magnetization to in-plane level, but it takes longer time to complete the reversal. Therefore, we also considered the SHE-assisted switching scheme where a small SHE current pulse creates a large angle and STT can quickly switch the magnetization reversal [21].

### D. Spin Hall Effect Efficiency

The spin Hall effect efficiency is defined as the spin polarization ratio, $P_{SHE}$, which depends on the geometry of SHM and MTJ as well as the bulk spin hall angle, $\theta_{SHE0}$ [22] [23].

$$
\begin{aligned}
P_{SHE} &= \frac{I_{spin}}{I_{charge}} = \frac{A_{MTJ}}{A_{SHM}} \cdot \frac{J_{MTJ}}{J_{SHM}} \\
&= \frac{A_{MTJ}}{A_{SHM}} \cdot \theta_{SHE0} \left(1 - sech\left(\frac{t_{SHM}}{\lambda_{SHM}}\right)\right)
\end{aligned}
\tag{8}
$$

$$
\theta_{SHE} = \frac{J_{MTJ}}{J_{SHM}} = \theta_{SHE0} \left(1 - sech\left(\frac{t_{SHM}}{\lambda_{SHM}}\right)\right)
\tag{9}
$$

Here, $A_{MTJ}$ ($A_{SHM}$) is the cross-sections of MTJ (SHM), $J_{MTJ}$ ($J_{SHM}$) is the current density in the MTJ (SHM). Spin Hall angle, $\theta_{SHE}$, is defined as the ratio between charge and spin current density in SHM, $\theta_{SHE0}$ is the bulk spin Hall angle, $t_{SHM}$ and $\lambda_{SHM}$ are the thickness and spin diffusion length of SHM, respectively. The trade-off between $\theta_{SHE}$ and the ratio $\frac{A_{MTJ}}{A_{SHM}}$ shown in Fig. 6 requires a geometry optimization.
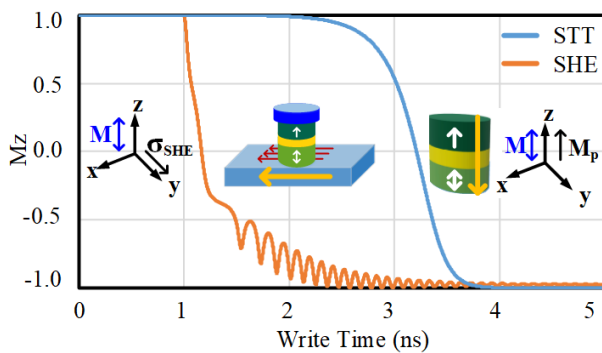


Fig. 5: PMTJ magnetization reversal with STT and SHE

### E. Composite Structure of SHE-MRAM

Several proposals have been made to switch PMTJ with SHE without the an external field [24]–[26]. While these proposals solve the field requirement, they still have challenges in fabrication, scaling or building a full-MTJ.

A simpler device with an in-plane magnetic layer (IPM) on top of the conventional MTJ as shown in Fig. 7 was proposed in [17]. The IPM layer of this composite structure provides the necessary field to deterministically switch the PMA free layer with SHE. In this work, both conventional and composite MTJ are modeled in SPICE.

A simplistic way to calculate the external field due to the stray field from IPM layer acting on the free-layer is to use magnetostatic potential method [27]. The expression of the magnets field in space becomes,

$$
\begin{aligned}
H_s(r) = &-\frac{1}{4\pi} \int \int \int d^3r' \Delta \cdot M(r') \frac{r-r'}{|r-r'|^3} \\
&+ \frac{1}{4\pi} \int \int d^2r' n' \cdot M(r') \cdot \frac{r-r'}{|r-r'|^3}
\end{aligned}
\tag{10}
$$

Here, $M$ is the magnetization direction, $M \cdot n$ is the source of demagnetization field, $r$ is the position vector of the point to measure the field, and $r'$ is the position vector of the point in the magnet. An IPM layer with dimension 100nm×50nm×7nm has an average stray field of 42mT inside the free layer with cross-section 45nm×45nm. The in-plane and out-of-plane components of $H_s$ are shown in Fig. 8 as $H_{sx}$ and $H_{sz}$. As $H_{sx}$ inside free-layer is very close to uniform, we assumed a uniform field of 40mT for simplicity.

### F. Effect of Temperature

The saturation magnetization, $M_s$, and polarization factor, $P$ are temperature dependent material parameters. The thermal

TABLE I: Universal SPICE Model Setup

| Properties | Equation parameter |
|---|---|
| In-plane magnetic anisotropy | $\mathbf{M}_p = [0, \pm 1, 0]$ |
| Perpendicular magnetic anisotropy | $\mathbf{M}_p = [0, 0, \pm 1]$ |
| STT switching | $\zeta_{STT} = f(J_{MTJ})$, $\zeta_{SHE} = 0$ |
| SHE switching | $\zeta_{SHE} = f(J_{SHM})$, $\zeta_{STT} = 0$, $\sigma_{SHE} = [0, \pm 1, 0]$ |
| SHE assisted STT switching | $\zeta_{STT} = f(J_{MTJ})$, $\zeta_{SHE} = f(J_{SHM})$, $\sigma_{SHE} = [0, \pm 1, 0]$ |
| Switching without external field | $\mathbf{H}_{eff} = \mathbf{H}_{eff0}$ |
| Switching with external field | $\mathbf{H}_{eff} = \mathbf{H}_{eff0} + \mathbf{H}_{app}$ |

stability factor and performances of MTJ depend on the system temperature as well [28].

$$M_s(T) = M_{s0}(1 - T/T_c)^\beta \quad (11)$$

$$P(T) = P_0(1 - \alpha_{sp}T^{3/2}) \quad (12)$$

Here, $M_{s0}$ and $P_0$ are the saturation magnetization and polarization factor at $0K$, respectively, $T_c$ is the Curie temperature, and $\beta$ and $\alpha_{sp}$ are material dependent empirical constants.

### G. Thermal Fluctuation

Previous macrospin models assumed a fixed initial angle which is a function of thermal stability factor, $\Delta$ [28]

$$\theta_{ini} = \sin^{-1}\frac{1}{(2\Delta)^{1/2}} \quad (13)$$

This fixed initial angle assumption overlooks the thermal fluctuation. The initial angle follows a Fokker-Plank distribution that produces a non-deterministic transient behavior. The distribution, $\rho_{initial}(\theta)$ is defined as follows [29] and shown in Fig. 9.

$$\rho_{initial}(\theta) = \frac{\exp(-\Delta \sin^2\theta)}{\int_0^\pi \sin\theta \exp(-\Delta \sin^2\theta)d\theta} \quad (14)$$

Here, $\Delta$ is the thermal stability factor. The switching probability for a fixed write current can be found by running a Monte-Carlo simulation of LLG equation with a set of initial angle sampled from (14) [30].

The Cartesian components of the random thermal field during the switching process follows independent Gaussian distributions with zero mean and standard deviation, $\sigma_{H_{th}}$.

$$\sigma_{H_{th}} = \sqrt{(2k_B\alpha T)/(\mu_0\gamma V M_s\delta t)} \quad (15)$$

Here, $k_B$ is the Boltzmann constant, $\mu_0$ is the permeability, $\gamma$ is the gyromagnetic ratio, and $\delta t$ is the time step.

### H. Tunnel Magnetoresistance (TMR)

The TMR of the MTJ is defined as $(R_{AP} - R_P)/R_p$ where $R_{AP}$ and $R_P$ are the anti-parallel and parallel resistances of MTJ, respectively. The TMR of the MTJ depends on voltage and temperature of the MTJ as follows [28]:

$$TMR(T,V) = \frac{2P_0^2(1 - \alpha_{sp}T^{3/2})^2}{1 - (1 - \alpha_{sp}T^{3/2})^2} \cdot \frac{1}{1 + (V/V_0)^2} \quad (16)$$

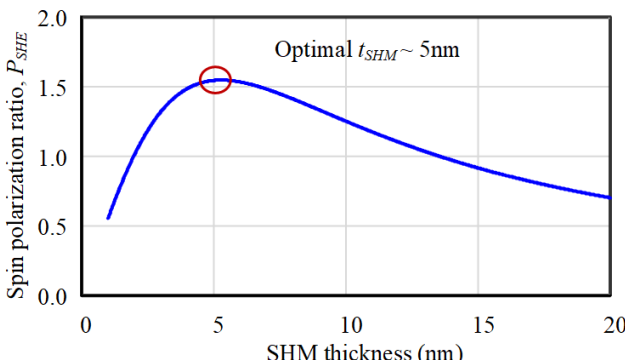Here, $V_0$ is another empirical fitting parameter.



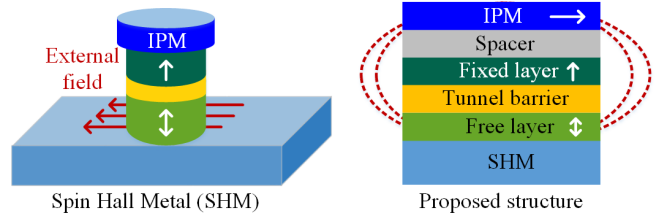Fig. 6: Effect of SHM thickness on spin polarization ratio



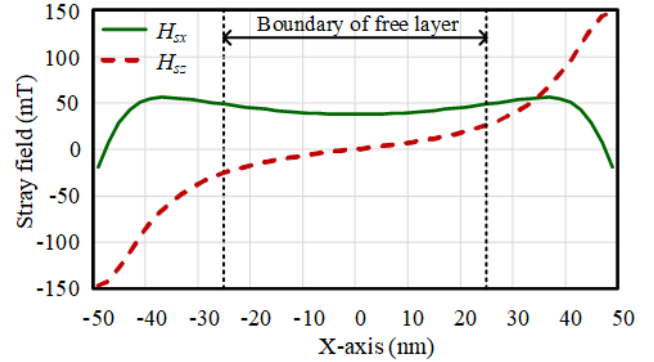Fig. 7: Composite MTJ to switch PMA with stray field [17]



Fig. 8: Stray field distribution in space

## III. SPICE MODEL FRAMEWORK

### A. Key Features

There have been a few compact MTJ models proposed in the past [31]–[34]. However, they required off-line calculations for geometry dependent effective anisotropy field and thus lacked the flexibility to study necessary scaling trends. A technology agnostic model was proposed in [16] [28] and solved some of these issues. However, the SHE-MRAM model proposed in [16] did not model the LLG equation for PMTJ. Moreover, the model lacked the geometry dependence of $\theta_{SHE}$.

We developed a SPICE model fulfilling all the aforementioned qualities. The list of user-defined input parameters are given in Table II. Our model has three main sub-circuits with basic circuit elements to capture the physics of MTJ, namely the resistance, heat diffusion, and the dynamic spin motion.

### B. Modes of Switching

With the comprehensive list of user-defined input, our model works for IPMTJ/PMTJ structures under a variety of MTJ switching scenarios, including STT switching/SHE switching, with/without field, etc. Here we focus on the switching of PMTJ, which is preferred for memory applications due to higher storage density, better thermal stability and lower power consumption [35]. Four typical switching schemes will be studied and compared, as shown in Fig. 11. The scheme (a) is STT-only switching, where the current goes through the MTJ. The scheme (b) is SHE-only switching in presence of a field, where the current goes through the SHM. The scheme (c) is SHE-assisted STT switching where SHE helps bringing the magnetization to in-plane level and STT completes the switching. Finally, scheme (d) is similar to scheme (c) except for an external field to provide additional tilt in the magnetization.
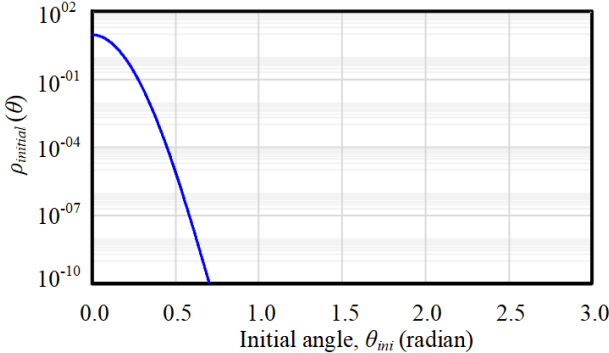
Fig. 9: Initial angle distribution



Fig. 11: Different write schemes: (a) STT-only, (b) SHE-only, (c) SHE-assisted STT (without field), and (d) SHE-assisted STT with field

The in-plane field in method (b) and (d) is generated by the in-plane layer of composite MTJ. It is worth noting that this effective external field may have some other sources as described in [24]–[26].

### C. Model Description

All of the components required to calculate the dynamics of magnetization as described in (5) are realized in SPICE with basic circuit elements and SPICE commands in different sub-circuits similarly to [28]. Hence, the compatibility with SPICE is ensured while solving mathematical problems regarding magnet physics. The internal calculations are performed by representing data as voltages and by using appropriate circuit relationship. For example, dependent sources were used to implement simple linear equations as in (7) that uses node voltages and branch currents as internal variables. Multiplications as in (6) were realized with a current source and resistor where current and resistors are the multiplicands, and the voltage across the resistance is the result. The differential LLG equation computation described in (5) was implemented using a voltage dependent current source with a capacitor in parallel. The MTJ temperature was implemented with a simple RC line model [33]. Three separate circuits were built to capture the three-dimensional vector information. The sub-circuits are then put together in one model file to combine the temperature and resistance of the system with the dynamic motion of spin.
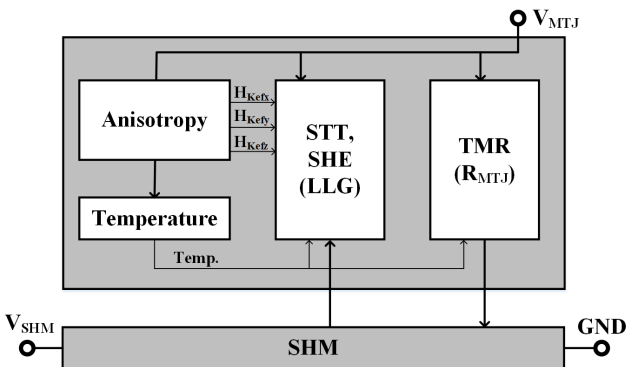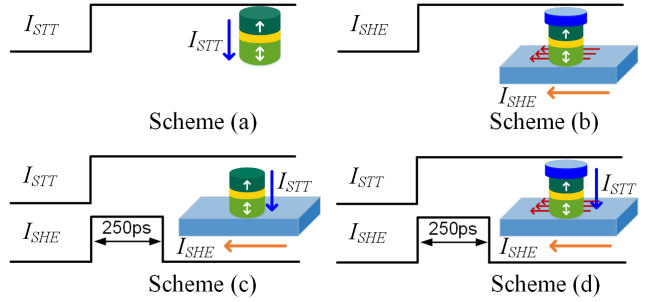
The initial angle of the MTJ plays a critical role in the switching mechanism. The model has two options for initial angle, $\theta_{ini}$. The default option is to use (13), and the other option is to use sampled data from the initial angle distribution described in (14) for Monte-Carlo simulation. Additionally, a random thermal field with Gaussian distribution with standard deviation described in (15) is added as a voltage source with the anisotropy field to emulate runtime stochasticity.

The framework is described in Fig. 10. Here, both SHE and STT are solved in the same LLG solver to accommodate the case where both effects are present. The applied field, either from an external source, or from an in-plane layer in the composite structure is another input to the model. The addition of applied field in the system provides additional flexibility to analyze the field assisted switching as well.

## IV. DESIGN AND PERFORMANCE ANALYSIS

We will divide this section in the following manner: we first describe the simulation setup for four different write schemes, and then the Monte-Carlo simulation based on initial angle distribution.

TABLE II: User-defined input parameters to SPICE model

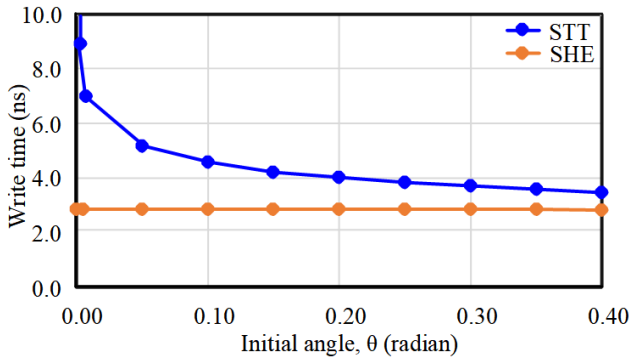| Input | Description |
|---|---|
| $W_m$ | MTJ Free layer width |
| $L_m$ | MTJ Free layer length |
| $t_m$ | MTJ Free layer thickness |
| $\alpha$ | Damping factor |
| $M_{s0}$ | Saturation magnetization ($0K$) |
| $P_0$ | Polarization factor ($0K$) |
| $T_0$ | Initial temperature |
| $RA$ | Resistance-area product |
| $K_u$ | Crystal anisotropy constant (CPMTJ) |
| $t_c$ | Critical thickness (IPMTJ) |
| $\theta_{ini}$ | Initial angle |
| $MA$ | IMA/PMA |
| $State$ | Initial magnetic state |
| $W_{SHM}$ | Spin Hall metal width |
| $L_{SHM}$ | Spin Hall metal length |
| $t_{SHM}$ | Spin Hall metal thickness |
| $\theta_{SHE0}$ | Bulk spin Hall angle |
| $\rho_{SHM}$ | SHM resistivity |
| $\lambda_{SHM}$ | SHM spin diffusion length |
| $H_{app}$ | External applied field |



Fig. 10: SPICE model framework

Fig. 12: Effect of initial angle on PMTJ switching time

### A. Simulation Setup

We have chosen a PMA SHE-MRAM with dimension 45nm $\times$ 45nm $\times$ 0.7nm with a $\Delta$ of 70 which corresponds to a 10 year retention time based on a memory size of 128 MB and failure probability of 0.01% [28]. The magnetic and geometric parameters of MTJ and SHM are listed in the Table III.

TABLE III: Material Parameters

| MTJ Parameters | |
|---|---|
| MTJ type | Crystalline perpendicular |
| MTJ material | FePdX |
| Free layer dimensions, $L_m \times W_m \times t_m$ | 45nm $\times$ 45nm $\times$ 0.7nm |
| Saturation magnetization constant, $M_s$ | 1185 emu/cc [28] |
| Crystal anisotropy constant, $K_u$ | $9 \times 10^6$ erg/cc [36] [28] |
| Thermal stability factor, $\Delta$ (85°C) | 70.5 |
| Damping constant, $\alpha$ | 0.02 [28] |
| Polarization factor, $P$ | 0.73 [28] |
| TMR ratio | 150 % |
| RA ($\Omega \cdot \mu m^2$) | 5 |
| SHM Parameters | |
| SHM dimensions, $L_{SHM} \times W_{SHM} \times t_{SHM}$ | 60nm $\times$ 45nm $\times$ 5nm |
| Bulk spin Hall angle, $\theta_{SHE0}$ | 0.4 [23] |
| SHM spin diffusion length, $\lambda_{SHM}$ | 3.5nm [23] |
| SHM resistivity, $\rho_{SHM}$ | 200 $\mu\Omega \cdot$ cm$^2$ |
| SHE spin polarization factor, $P_{SHE}$ | 1.55 |

We have analyzed four different schemes to write a PMA MTJ as shown in Fig. 11. The schemes are as follows:

- Scheme (a): STT-only switching
- Scheme (b): SHE-only switching (external field)
- Scheme (c): SHE-assisted STT switching (without field)
- Scheme (d): SHE-assisted STT switching (external field)

A traditional MRAM and MTJ structure was assumed for scheme (a) and scheme (c) switching while composite MTJ structure of Fig. 7 was assumed for the other two schemes.

### B. Monte-Carlo Simulation Results

The initial angle, $\theta_{ini}$, plays a vital role in the switching process of STT-MRAM. The switching time increases very fast with the decrease of $\theta_{ini}$ as shown in Fig. 12. We can explain this behavior from the LLG equation as described in (5). The Slonczewski term in the LLG equation depends on the magnitude of the cross product, $\mathbf{M} \times \mathbf{M}_p$. The magnitude of this term is tiny for small initial angle as it depends on the $\sin(\theta_{ini})$, where $\theta_{ini}$ is the angle between $\mathbf{M}$ and $\mathbf{M}_p$.

STT cannot begin the switching process if $\theta_{ini} = 0$. On the other hand, Fig. 12 also shows the initial angle does not affect the switching time of a SHE-MRAM significantly. The angle of interest for SHE is already very large and close to $\pi/2$ as evident from (5),. Hence, the small change in the initial angle is not very significant for SHE-MRAM.

We sampled 1000 initial angles from the probability density functions defined in (14) and ran Monte-Carlo simulation with a Gaussian random thermal field with $\sigma_{H_{th}}$ =9.2mT calculated using (15). The write time for both PMA STT-MRAM and SHE-MRAM are shown in Fig. 13. The STT and SHE currents used were $100\mu A$ and $400\mu A$, respectively. For scheme (b), the time to take the magnetization to bring down up to in-plane level was less than 1ns, but the complete reversal required a larger delay. The SHE current, $I_{SHE}$, was larger than STT current as the effective spin Hall angle, $\theta_{SHE}$ was only 0.22 using (9) and smaller $I_{SHE}$ could not complete the write operation for the external field of 40mT.

The Monte-Carlo simulation showed an intriguing result in favor of SHE-MRAM. Thermal fluctuation makes the write time of STT-MRAM somewhat non-deterministic for real life application, and to avoid write error, very large write time has to be used. On the other hand, the write time of SHE-MRAM is a very weak function of initial angle and is much more robust against thermal fluctuation. However, the write current required for SHE-only switching was very large. There are promising research initiatives going on to increase the bulk spin Hall angle, $\theta_{SHE0}$, which will potentially bring the switching time requirement down [37]. For all the subseqent simulations, we have taken $write\ time = mean + 6 \times standard\ deviation(\sigma)$ to emulate write error rate, $WER = 10^{-9}$.

The SHE-assisted STT switching described in Fig. 11 also showed similar benefit as SHE-only switching in Monte-Carlo simulation. However, the minimum SHE-current required to assist STT for schemes (c) and (d) were much smaller than SHE-only case. Fig. 14 shows the SHE-assisted STT write time with and without external field for 1000 Monte-Carlo simulations. Here, the $I_{STT}$ was $100\mu A$ and the external field in scheme (d) was 40mT. The results of scheme (b) show the SHE can assist STT even without any external field.

The write energy of STT-MRAM and SHE-MRAM cells including transistors for various write times for different write
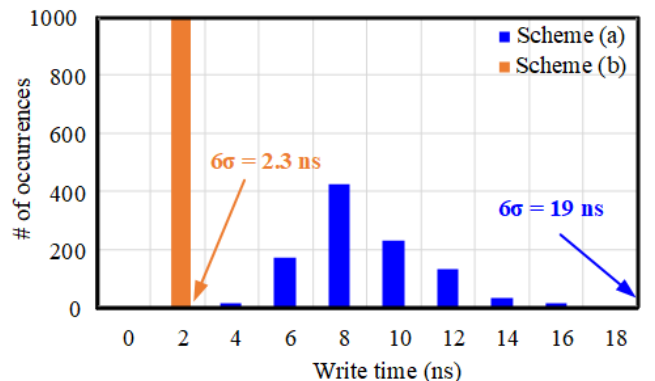


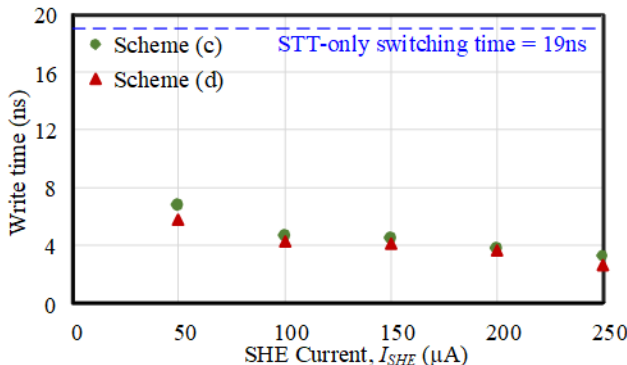Fig. 13: Switching time distribution for schemes (a) and (b)

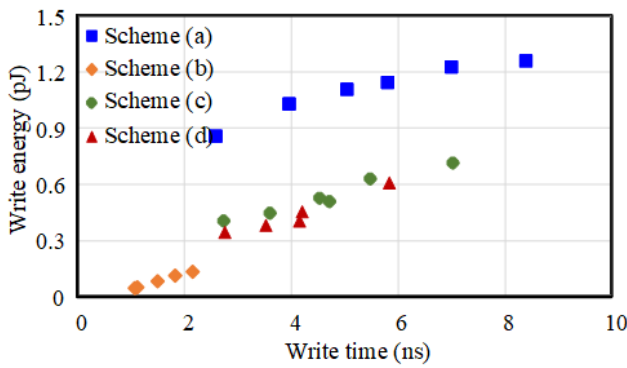Fig. 14: Effect of SHE current for schemes (c) and (d)



Fig. 15: Write energy for different write schemes

## V. CONCLUSION

We benchmarked various write schemes of STT-MRAM and SHE-MRAM using our universal SPICE model. Monte-Carlo simulation showed SHE is less susceptible to thermal fluctuation than STT. SHE-only switching also showed a $8\times$ and $7\times$ delay and energy reduction, respectively. However, this scheme required a large write current of $400\mu$A. SHE-assisted STT switching showed $2\times$ and $3\times$ delay and energy reduction, respectively, with a 250ps SHE current pulse of $50\mu$A. These results indicate SHE-assisted STT scheme can be a viable candidate for embedded applications.

## ACKNOWLEDGMENT

currents are shown in Fig. 15. We have assumed the voltage across the memory cell is the system $V_{DD} = 1.0V$. The write energy is beneficiary for SHE-only switching. However, the SHE-only switching requires a large current which may prohibitively increase the access transistor size. SHE-assisted STT switching can also reduce the energy and delay requirement with a smaller overhead.

The current, delay and energy of various write schemes are shown in Table IV. As the scaling trend requires small write current, we considered STT-only switching with $100\mu$A as the base case. SHE-only switching showed the largest energy and delay reduction with a large SHE current. On the other hand, SHE-assisted STT switching of scheme (c) and scheme (d) showed $2\times$ and $3\times$ reduction in delay and energy, respectively. However, scheme (d) requires a composite structure similar to scheme (b). The small current overhead of scheme (c) and (d) make SHE-assisted STT a viable option for memory operation.

TABLE IV: Write current and delay for various schemes

| Write scheme | | (a) | (b) | (c) | (d) |
|---|---|---|---|---|---|
| External field | | N/A | 40mT | N/A | 40mT |
| Write current | $I_{STT}$ | $100\mu$A | 0 | $100\mu$A | $100\mu$A |
| | $I_{SHE}$ | 0 | $400\mu$A* | $50\mu$A | $50\mu$A |
| Delay reduction | | $1\times$ | $8.3\times$ | $1.8\times$ | $2.3\times$ |
| Energy reduction | | $1\times$ | $6.8\times$ | $2.8\times$ | $3.2\times$ |

*large write current was required

## REFERENCES

[1] B. Behin-Aein, *et al.*, "Proposal for an all-spin logic device with built-in memory," *Nature Nanotechnology*, vol. 5, pp. 266–270, Apr 2010.
[2] J. A. Currivan, *et al.*, "Low energy magnetic domain wall logic in short, narrow, ferromagnetic wires," *IEEE Magnetics Letters*, vol. 3, pp. 3000104–3000104, 2012.
[3] R. P. Cowburn *et al.*, "Room temperature magnetic quantum cellular automata," *Science*, vol. 287, no. 5457, pp. 1466–1468, 2000.
[4] A. Lyle, *et al.*, "Direct communication between magnetic tunnel junctions for nonvolatile logic fan-out architecture," *Applied Physics Letters*, vol. 97, no. 15, p. 152504, 2010.
[5] M. Hosomi, *et al.*, "A novel nonvolatile memory with spin torque transfer magnetization switching: spin-RAM," in *IEEE International Electron Devices Meeting (IEDM)*, pp. 459–462, Dec 2005.
[6] J. P. Kim, *et al.*, "A 45nm 1Mb embedded STT-MRAM with design techniques to minimize read-disturbance," in *Symposium on VLSI Circuits*, pp. 296–297, June 2011.
[7] K. Lee *et al.*, "Development of embedded STT-MRAM for mobile system-on-chips," *IEEE Transactions on Magnetics*, vol. 47, pp. 131–136, Jan 2011.
[8] J.-P. Wang, *et al.*, "Magnetic tunnel junction based integrated logics and computational circuits," *Nanomagnetic and Spintronic Devices for Energy-Efficient Memory and Computing*, p. 133, 2016.
[9] J.-P. Wang, *et al.*, "Spin transfer torque random access memory," *Emerging Nanoelectronic Devices*, 2014.
[10] S. A. Wolf, *et al.*, "The promise of nanomagnetics and spintronics for future logic and universal memory," *Proceedings of the IEEE*, vol. 98, pp. 2155–2168, Dec 2010.
[11] S. W. Chung, *et al.*, "4Gbit density STT-MRAM using perpendicular MTJ realized with compact cell structure," in *IEEE International Electron Devices Meeting (IEDM)*, pp. 27.1.1–27.1.4, Dec 2016.
[12] Y. J. Song, *et al.*, "Highly functional and reliable 8Mb STT-MRAM embedded in 28nm logic," in *IEEE International Electron Devices Meeting (IEDM)*, pp. 27.2.1–27.2.4, Dec 2016.
[13] K. C. Chun, *et al.*, "A scaling roadmap and performance evaluation of in-plane and perpendicular MTJ based STT-MRAMs for high-density cache memory," *IEEE Journal of Solid-State Circuits*, vol. 48, pp. 598–610, Feb 2013.
[14] L. Liu, *et al.*, "Current-induced switching of perpendicularly magnetized magnetic layers using spin torque from the spin Hall effect," *Phys. Rev. Lett.*, vol. 109, p. 096602, Aug 2012.
[15] L. Liu, *et al.*, "Spin-torque switching with the giant spin Hall effect of Tantalum," *Science*, vol. 336, no. 6081, pp. 555–558, 2012.
[16] J. Kim, *et al.*, "Spin-Hall effect MRAM based cache memory: A feasibility study," in *Device Research Conference (DRC)*, pp. 117–118, June 2015.
[17] A. Klemm Smith, *et al.*, "External field free spin Hall effect device for perpendicular magnetization reversal using a composite structure with biasing layer," *ArXiv e-prints*, Feb. 2016.

[18] S. Ikeda, *et al.*, "A perpendicular-anisotropy CoFeBMgO magnetic tunnel junction," *Nat. Mater.*, vol. 9, pp. 721–724, September 2010.

[19] I. M. Miron, *et al.*, "Perpendicular switching of a single ferromagnetic layer induced by in-plane current injection," *Nature*, vol. 476, no. 7359, 2011.

[20] Z. Zhao, *et al.*, "Spin Hall switching of the magnetization in Ta/TbFeCo structures with bulk perpendicular anisotropy," *Applied Physics Letters*, vol. 106, no. 13, p. 132404, 2015.

[21] A. van den Brink, *et al.*, "Spin-Hall-assisted magnetic random access memory," *Applied Physics Letters*, vol. 104, no. 1, p. 012403, 2014.

[22] S. Manipatruni, *et al.*, "Energy-delay performance of giant spin Hall effect switching for dense magnetic memory," *Applied Physics Express*, vol. 7, no. 10, p. 103001, 2014.

[23] Q. Hao *et al.*, "Giant spin Hall effect and switching induced by spin-transfer torque in a $W/Co_{40}Fe_{40}B_{20}/MgO$ structure with perpendicular magnetic anisotropy," *Phys. Rev. Applied*, vol. 3, 2015.

[24] G. Yu, *et al.*, "Switching of perpendicular magnetization by spin-orbit torques in the absence of external magnetic fields," *Nat Nano*, vol. 9, pp. 548–554, Jul 2014. Article.

[25] L. You, *et al.*, "Switching of perpendicularly polarized nanomagnets with spin orbit torque without an external magnetic field by engineering a tilted anisotropy," *Proceedings of the National Academy of Sciences*, vol. 112, no. 33, pp. 10310–10315, 2015.

[26] S. Fukami, *et al.*, "Magnetization switching by spin-orbit torque in an antiferromagnet-ferromagnet bilayer system," *Nat. Mater.*, vol. 15, pp. 535–541, May 2016. Article.

[27] R. C. O'Handley, *Modern Magnetic Material- Principles and Applications*. Wiley, 1999.

[28] J. Kim, *et al.*, "A technology-agnostic MTJ SPICE model with user-defined dimensions for STT-MRAM scalability studies," in *IEEE Custom Integrated Circuits Conference (CICC)*, pp. 1–4, Sept 2015.

[29] W. H. Butler, *et al.*, "Switching distributions for perpendicular spin-torque devices within the macrospin approximation," *IEEE Transactions on Magnetics*, vol. 48, pp. 4684–4700, Dec 2012.

[30] P. Bonhomme, *et al.*, "Circuit simulation of magnetization dynamics and spin transport," *IEEE Transactions on Electron Devices*, vol. 61, pp. 1553–1560, May 2014.

[31] J. D. Harms, *et al.*, "SPICE macromodel of spin-torque-transfer-operated magnetic tunnel junctions," *IEEE Transactions on Electron Devices*, vol. 57, pp. 1425–1430, June 2010.

[32] Z. Xu, *et al.*, "Compact modeling of STT-MTJ for SPICE simulation," in *Proceedings of the European Solid-State Device Research Conference (ESSDERC)*, pp. 338–341, Sept 2013.

[33] G. D. Panagopoulos, *et al.*, "Physics-based SPICE-compatible compact model for simulating hybrid MTJ/CMOS circuits," *IEEE Transactions on Electron Devices*, vol. 60, pp. 2808–2814, Sept 2013.

[34] S. Manipatruni, *et al.*, "Vector spin modeling for magnetic tunnel junctions with voltage dependent effects," *Journal of Applied Physics*, vol. 115, no. 17, p. 17B754, 2014.

[35] M. Wang, *et al.*, "Tunnel junction with perpendicular magnetic anisotropy: Status and challenges," *Micromachines*, vol. 6, no. 8, pp. 1023–1045, 2015.

[36] T. Ichitsubo, *et al.*, "Control of c-axis orientation of 110-fepd in dual-phase-equilibrium fepd/fe thin films," *Journal of Applied Physics*, vol. 109, no. 3, p. 033513, 2011.

[37] M. DC, *et al.*, "Room-temperature perpendicular magnetization switching through giant spin-orbit torque from sputtered bixse(1-x) topological insulator material," *ArXiv e-prints*, 2017.

PLACE PHOTO HERE

**Ibrahim Ahmed** is currently pursuing Ph.D. degree in Electrical Engineering at the University of Minnesota, Twin Cities, Minnesota. He received B.Sc. in Electrical and Electronic Engineering from Bangladesh University of Engineering and Technology (BUET), Dhaka, Bangladesh in 2013. His research focuses on designing and optimizing beyond CMOS devices and architectures, especially sprintornic logic and memory devices, modeling of spin based memories as well as all spin logic based on Heusler alloy.

PLACE PHOTO HERE

**Zhengyang Zhao** is currently pursuing the Ph.D. degree in Electrical Engineering at the University of Minnesota, Minneapolis, MN. He received the B.S. degree in Electrical Engineering from Xi'an Jiaotong University, China, in 2012. His research focuses on development of novel spintronic devices to implement energy-efficient logic and memory devices. His recent work includes studying spin-orbit torque induced nano-magnet switching, voltage control of magnetization reversal using piezoelectric strain, and voltage control of exchange bias using magnetoelectric materials.

PLACE PHOTO HERE

**Meghna G. Mankalale** received her B.E. degree from Visvesvaraya Technological University, India in 2007. She worked as a Research and Development Engineer in IBM, India from 2007 to 2013. She is currently pursuing her PhD in the Department of Electrical and Computer Engineering at the University of Minnesota. Her research interests include design and optimization of devices in beyond CMOS technologies, particularly in the area of Spintronics.

PLACE PHOTO HERE

**Sachin S. Sapatnekar** is the Henle Chair in ECE and the Distinguished McKnight University Professorship at the University of Minnesota. He received his PhD from the University of Illinois at Urbana-Champaign in 1992. He is a recipient of the NSF Career Award, seven Best Paper awards, the IC-CAD Ten Year Retrospective Most Influential Paper Award (twice), the SRC Technical Excellence award, and the SIA University Research Award. He is a Fellow of the IEEE and the ACM. He served on the Executive Committee of the ACM/IEEE Design Automation Conference (DAC) from 2005-2011, including as General Chair in 2010, and was Editor-in-Chief of the IEEE Transactions on CAD from 2010-2013. He is an author of over 300 publications in the area of design automation of CMOS-based and emerging integrated systems.

PLACE PHOTO HERE

**Jian Ping Wang** is the Robert Hartman Chair and a Distinguished McKnight University Professor of Electrical and Computer Engineering, and a member of the graduate faculty in Physics and Chemical Engineering at the University of Minnesota. Dr. Wang is the director of the Center for Spintronic Materials, Novel Interfaces and Architectures (C-SPIN), one of six centers of STARnet program. He established and managed the Magnetic Media and Materials program at the Data Storage Institute, Singapore, as the founding program manager, from 1998 to 2002. He received the INSIC technical award in 2006 for his pioneering work in exchange coupled composite magnetic media. He has authored and co-authored more than 300 publications in peer-reviewed top journals and conferences and holds 56 patents (issued and pending). His current research programs focus on searching, fabricating and fundamentally understanding new nanomagnetic and spintronic materials and devices. His inventions have been used in today's hard disk drive and STT-RAM. He was the first to demonstrate the perpendicular spin transfer torque device and the most fast switching of a thermally stable MTJ. He has been performing pioneering research on magnetic tunnel junction based logic devices.

PLACE
PHOTO
HERE

**Chris H. Kim** Chris H. Kim received his B.S. and M.S. degrees from Seoul National University and a Ph.D. degree from Purdue University. He joined the electrical and computer engineering faculty at the University of Minnesota, Minneapolis, MN, in 2004 where he is currently a professor. Prof. Kim is the recipient of an SRC Technical Excellence Award, a Council of Graduate Students Outstanding Faculty Award, an NSF CAREER Award, a Mcknight Foundation Land-Grant Professorship, a 3M Non-Tenured Faculty Award, DAC/ISSCC Student Design Contest Awards, IBM Faculty Partnership Awards, an IEEE Circuits and Systems Society Outstanding Young Author Award, and ISLPED Low Power Design Contest Awards. He is an author/coauthor of 200+ journal and conference papers and has served as the technical program committee chair for the 2010 International Symposium on Low Power Electronics and Design (ISLPED). His research interests include digital, mixed-signal, and memory circuit design in silicon and non-silicon (organic TFT and spin) technologies.